ARTICLE INFORMATION

Received: 14 December 2012 | Revised: 24 January 2013 | Accepted: 31 January 2013

doi: 10.1259/bjr.20120653

Cite this article as:
Nilsson H, Blomqvist L, Douglas L, Nordell A, Janczewska I, Näslund E, et al. Gd-EOB-DTPA-enhanced MRI for the assessment of liver function and volume in liver cirrhosis. Br J Radiol 2013;86:20120653.

Gd-EOB-DTPA-enhanced MRI for the assessment of liver function and volume in liver cirrhosis

[1]H NILSSON, MD, PhD, [2,3]L BLOMQVIST, MD, PhD, [4]L DOUGLAS, MSc, PhD, [4]A NORDELL, MSc, [5]I JANCZEWSKA, MD, PhD, [1]E NÄSLUND, MD, PhD and [1]E JONAS, MD, PhD

[1]Division of Surgery, Department of Clinical Sciences, Danderyd Hospital, Karolinska Institutet, Stockholm, Sweden
[2]Department of Diagnostic Radiology, Karolinska University Hospital, Solna, Stockholm, Sweden
[3]Department of Molecular Medicine and Surgery, Karolinska Institutet, Stockholm, Sweden
[4]Department of Medical Physics, Karolinska University Hospital, Solna, Stockholm, Sweden
[5]Division of Internal Medicine, Department of Clinical Sciences, Danderyd Hospital, Karolinska Institutet, Stockholm, Sweden

Address correspondence to: Dr Henrik Nilsson
E-mail: *henrik.nilsson@ki.se*

Objective: The aims of this study were to use dynamic hepatocyte-specific contrast-enhanced MRI to evaluate liver volume and function in liver cirrhosis, correlate the results with standard scoring models and explore the inhomogeneous distribution of liver function in cirrhotic livers.

Methods: 10 patients with liver cirrhosis and 20 healthy volunteers, serving as controls, were included. Hepatic extraction fraction (HEF), input relative blood flow and mean transit time were calculated on a voxel-by-voxel basis using deconvolutional analysis. Segmental and total liver volumes as well as segmental and total hepatic extraction capacity, expressed in HEFml, were calculated. An incongruence score (IS) was constructed to reflect the uneven distribution of liver function. The Mann–Whitney *U*-test was used for group comparison of the quantitative liver function parameters, liver volumes and ISs. Correlations between liver function parameters and clinical scores were assessed using Spearman rank correlation.

Results: Patients had larger parenchymal liver volume, lower hepatocyte function and more inhomogeneous distribution of function compared with healthy controls.

Conclusion: The study demonstrates the non-homogeneous nature of liver cirrhosis and underlines the necessity of a liver function test able to compensate for the heterogeneous distribution of liver function in patients with diseased liver parenchyma.

Advances in knowledge: The study describes a new way to quantitatively assess the hepatic uptake of gadoxetate or gadolinium ethoxybenzyl diethylenetriaminepentaacetic acid in the liver as a whole as well as on a segmental level.

In patients undergoing liver resection, post-operative liver failure is a major concern and has in current practice become the biggest cause for mortality after liver resection [1–3]. Residual liver should be of adequate volume and quality to sustain immediate post-operative function and to allow regeneration for complete restoration of hepatic function. Currently, surgical decision-making is predominantly based on volume calculation from cross-sectional imaging, sometimes in combination with liver function evaluation [4,5]. A variety of different methods for quantitative assessment of global liver function are available, including clearance–retention tests, redox chemistry and scintigraphy [6,7]. All currently available metabolic tests give a global assessment of liver function and do not account or correct for the possible heterogeneous distribution of function within the liver parenchyma. Scoring models, of which the Child–Pugh score (CPS) [8,9] and the model for end-stage liver disease (MELD) [10] are the most frequently used, are hampered by the same limitations.

A number of published studies, using different scintigraphic methods, have verified the presence of heterogeneous distribution of function in the liver parenchyma. In a group of patients with diverse underlying liver pathologies investigated with ^{99m}Tc-mebrofenin, it was found that liver function was unevenly distributed within the liver [11]. Regional variations in uptake were also demonstrated using ^{99m}Tc-labelled galactosyl human serum albumin [12,13]. This phenomenon was also observed in patients with primary sclerosing cholangitis using ^{99m}Tc-HIDA [14].

Gadoxetate or gadolinium ethoxybenzyl diethylenetriaminepentaacetic acid (Gd-EOB-DTPA; Primovist®, Bayer Healthcare, Berlin) is a contrast agent developed for MRI. It is a gadolinium chelate that is actively taken up into the hepatocytes through the organic anion-transporting polypeptides [15]. This is a property Gd-EOB-DTPA shares with the iminodiacetic acid compounds used in hepatobiliary scintigraphy (HBS) and with indocyanine green (ICG) [16–20]. Pharmacokinetic studies show that about 50% of the administered dose of Gd-EOB-DTPA is extracted by the liver and eliminated through the hepatobiliary pathway. The remaining 50% is eliminated by renal excretion [21]. As the hepatic elimination of Gd-EOB-DTPA is dependent on the integrity of the hepatocyte mass, quantification of the uptake should represent the same aspects of liver function as assessed by ICG clearance or HBS.

Dynamic hepatocyte-specific contrast-enhanced MRI (DHCE-MRI) has previously been used in animal models for the evaluation of hepatic function in various experimental settings, either using semi-quantitative parameters or using deconvolutional analysis (DA) [22–25]. In human studies, liver parenchymal enhancement after administration of Gd-EOB-DTPA has been shown to correlate with ICG clearance and with liver cirrhosis as assessed by the CPS [26,27], and subsequent biliary excretion has been shown to be delayed in patients with impaired liver function [28]. In a study of patients with primary biliary cirrhosis, quantitative parameters indicative of liver function derived from DA were shown to correlate with disease severity [29]. Also, compartmental modelling has been used to assess the hepatic uptake of Gd-EOB-DTPA, and the parameters derived were shown to be dependent on the CPS [30]. These findings support the hypothesis that results from DHCE-MRI have the potential to assess liver function.

The present study should be regarded as a feasibility study aiming to investigate DHCE-MRI as a method to explore the inhomogeneous distribution of liver function in patients with liver cirrhosis compared with a control group and to explore the correlation between DHCE-MRI-derived liver function parameters with commonly used clinical scoring models. The primary outcome was the overall hepatic extraction capacity of Gd-EOB-DTPA, and secondary outcomes were measures of liver function heterogeneity, liver function indices and correlation analysis.

METHODS

Study subjects

10 patients with varying degrees of alcohol- and/or viral hepatitis-induced liver cirrhosis were included in the study. The patients were regularly seen as outpatients participating in a screening programme for hepatocellular carcinoma (HCC) or had a history of liver decompensation requiring hospitalisation. Patients in the age group from 18 to 65 years were regarded eligible for participation. Patients with previous liver surgery apart from cholecystectomy, impaired renal function [glomerular filtration rate (GFR)$<30\,\mathrm{ml\,min^{-1}\,1.73\,m^{-2}}$] or contraindications for MRI were excluded. Image data from

20 healthy volunteers examined in the previous study were used as controls and recalculated according to the protocol in this study [31]. The controls had no history of hepatobiliary disease, previous hepatobiliary surgery or alcohol abuse. Written informed consent was obtained from all participants prior to examination and the study was approved by the Regional Ethical Review Board in Stockholm. For patients, relevant demographic and clinical data were documented, as well as results of serum liver function tests from the visit closest to the MR examination, date as documented in their clinical charts. The CPS and MELD scores were calculated for each patient [32,33]. The demographic and clinical parameters of the study subjects are summarised in Table 1 and the disease characteristics of the patients are summarised in Table 2.

MR procedure

All subjects were instructed to fast for at least 4 h prior to the examination. MRI was performed using a 1.5 T scanner (Intera; Philips Medical Systems, Best, Netherlands), with a Philips four-channel sensitivity encoding (SENSE) body coil. The dynamic contrast-enhanced sequence was performed using a T_1 weighted three-dimensional spoiled gradient-echo sequence (repetition time/echo time/flip angle 4.1 ms/2.0 ms/10°, field of view (FOV)=415 mm, acquisition matrix resolution 192×192, reconstruction matrix 256×256, 40 slices, slice thickness 10 mm with 5 mm overlap and SENSE factor R=2). Each volume was examined in a single breath-hold (12 s scan time per acquired volume) and the subjects were asked to hold their breath at the same depth during each acquisition. Three volumes were acquired pre-contrast for baseline calculations followed by repetitive sampling with step-wise increase in sampling intervals up to a total sampling time of 45 min. The control group was previously examined with an identical study protocol, although it used a total sampling time of 90 min. In this study, however, only the volumes acquired up to 45 minutes post-contrast injection were used in the analysis. The sampling time points, imaging parameters and data acquisition were thus identical in the two groups. A dose of 0.1 ml per kg Gd-EOB-DTPA 0.25 mmol ml^{-1} was injected into the anterior cubital vein, coinciding with the start of the fourth acquired volume. The contrast was injected using a power injector (Medrad® Spectris Solaris® EP MR Injection System, Medrad, Pittsburgh, PA), at an infusion rate of 2 ml s^{-1}, followed immediately by a bolus of 20 ml of saline (NaCl 0.9%) at the same infusion rate.

Image analysis

Segments were anatomically defined and the anatomical nomenclature adhered to as proposed by Strasberg [34,35]. Segment IV was subdivided into IVa and IVb. The horizontal intersegmental plane was defined as being at the level of the division of the portal vein into the left and right portal branches. Half of the voxels in this plane were regarded as representative of the superior segments (II, IVa, VII and VIII) and the other half

Table 1. Study subject characteristics

	Patients (n=10)	Controls (n=20)	
Gender (males/females)	8/2	10/10	
Age (years)	55.8±5.3	33.2±6.8	
			Reference
Bilirubin (μmol l^{-1})	35.1±23 (10)	12.6±5 (9)	<26
Albumin (g l^{-1})	32±8 (10)	42±2 (19)	36–48
Creatinine (μmol l^{-1})	91±23 (10)	83±17 (19)	<100 (males) and <90 (females)
PK-INR (INR)	1.37±0.3 (10)	1.1±0.1 (19)	<1.2
ALP (μkat l^{-1})	2.28±1.04 (10)	1.04±0.46 (19)	<1.9
ALT (μkat l^{-1})	0.97±0.69 (10)	0.41±0.26 (20)	<1.20 (males) and <0.76 (females)
AST (μkat l^{-1})	1.47±1.13 (10)	0.32±0.08 (20)	<0.76 (males) and <0.61 (females)

ALP, alkaline phosphatase; ALT, alanine aminotransferase; AST, aspartate aminotransferase; PK-INR, prothrombin complex-international normalised ratio.
Results are presented as mean ± SD, and numbers within brackets denote number of observations.

Table 2a. Disease characteristics of patients

	Median	Min	Max
MELD	13	6	19
CPS	7	5	12

CPS, Child–Pugh score; MELD, model for end-stage liver disease; max, maximum; min, minimum

Table 2b. Disease characteristics of patients

Child–Pugh class	*n*
A	4
B	5
C	1

as part of the inferior segments (III, IVb, V and VI). From a seed point placed in the inferior vena cava, lines were drawn in the plane of the right hepatic vein, the middle hepatic vein and the falciform ligament/umbilical fissure creating the vertical intersectional planes. This segmentation originating from the seed point is visualised by the blue lines shown in Figure 1. Segment I was manually outlined in every slice where it was visible according to the anatomical landmarks as described by Dodds et al [36]. In hepatobiliary phase images, where there is a high soft-tissue contrast resolution between liver parenchyma and surrounding tissues, the liver contour was manually outlined in every slice in a caudal-cranial fashion, excluding the major hilar structures. The manual outlining of the liver contour and segmentation was done by one person (first author) for both controls and patients. The volumes of the voxels within the defined borders were added to obtain total and segmental liver volumes for each subject. The voxel volume, determined by the FOV, slice thickness and in-plane spatial resolution parameters defined above, was approximately 13 mm^3 (1.6×1.6×5 mm). Relative signal intensity in the voxels was calculated by the logarithmic ratio expressed in Equation 1:

$$SI_r(t,\rho) = \ln\left(\frac{S(t,\rho)}{S_0(\rho)}\right) \quad (1)$$

where $SI_r(t, \rho)$ is the relative signal intensity at time t in voxel ρ; $S_0(\rho)$ is the mean image intensity in voxel ρ from the pre-contrast images, *i.e.* baseline signal intensity; and $S(t, \rho)$ is the measured image intensity in voxel ρ at time t. Image analysis and subsequent calculations were performed using in-house software written in MATLAB® (Mathworks, Natick, MA).

Figure 1. Parametric maps of quantitative liver function parameters. T_1 weighted spoiled gradient-echo images from a patient (top row) and healthy control (bottom row) where the results of the voxel-based quantitative liver function analysis are superimposed, colour-coded, on the anatomical images and presented as parametric maps are shown. The patient in the top row had the Child–Pugh score of 6 and model for end-stage liver disease score 11. The images in the middle column show input-relative blood flow (irBF) maps (perfusion) where the vascular structures are easily identified with a markedly higher irBF compared with the liver parenchyma. HEF, hepatic extraction fraction; MTT, mean transit time.

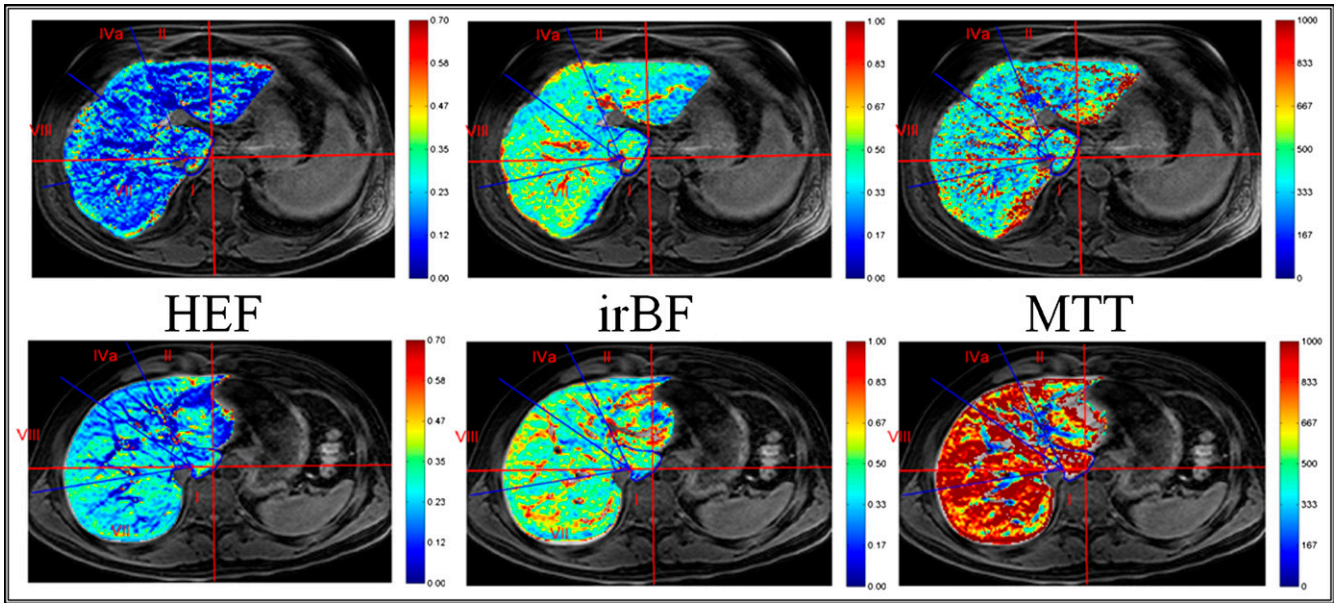

Liver function parameters

A quantitative assessment of liver function parameters was obtained using DA. With knowledge of the input function, *i.e.* the vascular inflow of contrast agent, and parenchymal response function, the impulse response function can be estimated through DA. The impulse response function is a mathematical representation of what the parenchymal response would be if the contrast agent had been delivered into the liver as an infinitely short bolus without subsequent recirculation. From the impulse response curve, several functional characteristics of the system can be derived, in this case the hepatic extraction fraction (HEF), input-relative blood flow (irBF) and mean transit time (MTT), as has been described extensively in earlier publications [29,31]. In this study, both mathematical methods described for DA in DHCE-MRI, the Fourier method with an appended tail and the matrix method using truncated singular value decomposition, were used. HEF was first described in HBS as a measurement of hepatic extraction efficiency, and it was defined as the proportion of tracer that is extracted by the liver in a single passage without tracer recirculation [37]. The irBF describes the peak blood flow in a defined volume relative to the peak blood flow in the input function, and is therefore a measurement of perfusion. MTT describes the mean time it takes for a unit of the tracer, or the contrast agent in this study, to pass through the system, in this case exiting either through vascular wash-out or excretion into the bile ducts. These parameters (HEF, irBF and MTT) were calculated in every voxel within the defined liver boundaries. The relative signal intensity-over-time in a voxel was regarded as the parenchymal response function, and the input function was defined by a region of interest (ROI) placed in the spleen. To ensure that the ROI in the spleen was truly representative of the blood content over the entire acquisition period, it was manually adjusted when needed. Based on findings in earlier studies and methodological considerations, voxels with HEF above 0.7 or irBF above 1 were regarded as artefacts and omitted from subsequent analysis [29,31]. Voxels representing vascular structures could be expected to have high perfusion, *i.e.* high irBF values. Therefore, upon completion of calculation of irBF for all voxels, an irBF threshold was defined by visual inspection in every subject that excluded major intrahepatic vessels without loss of parenchymal voxels. These vascular voxels were excluded from analysis of parenchymal properties. The final results thus yielded total and segmental parenchymal liver volumes with the exclusion of vessel volume. The high irBF in vascular structures is illustrated in Figure 1. Total liver function was defined as the total hepatocyte extraction capacity of Gd-EOB-DTPA and was expressed as HEFml. This parameter was obtained by adding the individual HEF of all parenchymal voxels (after the omission of vascular tissue) within the liver boundaries. For every segment, the functional capacity was obtained in a similar fashion, adding all parenchymal voxels within the predefined segmental borders. To assess the discrepancies regarding the segmental contribution of function and volume to the total liver function and volume, *i.e.* the heterogeneity of liver function distribution, an incongruence score (IS) was calculated for every segment as described in Equation 2:

$$\mathrm{IS} = \frac{\left[\left(\frac{Sn_\mathrm{f}}{T_\mathrm{f}}\right) - \left(\frac{Sn_\mathrm{v}}{T_\mathrm{v}}\right)\right]^2}{\left(\frac{Sn_\mathrm{v}}{T_\mathrm{v}}\right)} = \frac{(O-E)^2}{E}, \qquad (2)$$

where Sn_f is the functional capacity expressed as HEFml in segment n, T_f is the total liver functional capacity expressed as HEFml, Sn_v is the volume of segment n and T_v is the total liver volume. For each study subject, a total IS was obtained by the sum of the IS for each segment. Global median HEF, irBF and MTT were obtained by calculating the median of all parenchymal voxels within the liver boundaries.

Statistical analysis

Descriptive statistics using mean or median (with standard deviation and range) as appropriate were used to present clinical characteristics of the study subjects and the quantitative liver function parameters. Non-parametric tests (Mann–Whitney *U*-test and Wilcoxon matched-pairs signed-rank test) were used for group comparison of the quantitative liver function parameters, liver volumes and ISs. Correlations between liver function parameters and clinical scores were assessed using Spearman rank correlation. The significance threshold was set to $\alpha = 0.05$. STATA™ 10 (StataCorp, College Station, TX) was used for the statistical analyses.

RESULTS

The results of liver volume measurements and of the quantitative functional parameters are shown in Table 3. There were no differences regarding total liver

Table 3. Results of liver function and volume analysis

	Controls		Patients		*p*-value[a]
	Median (mean)	Min–max; SD	Median (mean)	Min–max; SD	
Total liver volume (ml)	1496 (1468)	1037–1934; 261	1577 (1593)	1357–1886; 196	$p=0.29$
Parenchymal volume (ml)	1256 (1267)	915–1692; 229	1435 (1473)	1225–1774; 200	$p<0.05$[a]
Total functional capacity (HEFml)	283 (286)	112–412; 73	171 (190)	53–341; 97	$p<0.05$[a]
Global median HEF	0.22 (0.22)	0.11–0.28; 0.04	0.09 (0.10)	0.02–0.20; 0.07	$p<0.05$[a]
Global median irBF	0.52 (0.52)	0.43–0.63; 0.05	0.48 (0.49)	0.31–0.74; 0.12	$p=0.17$
Global median MTT	789 (773)	477–1318; 223	453 (455)	203–686; 137	$p<0.05$[a]

HEF, hepatic extraction fraction; irBF, input-relative blood flow; max, maximum; min, miniumum; MTT, mean transit time; SD, standard deviation.
[a]Mann–Whitney *U*-test.

volume, but, when the vascular voxels were subtracted, the patient group had a statistically significant larger parenchymal volume, despite the fact that the overall parenchymal function, expressed as HEFml, was lower. Also, the median liver HEF was lower among patients, indicating lower parenchymal functional capacity. The median MTT was shorter in the patient group but perfusion, assessed as irBF, did not differ between the groups. However, a substantial variation in irBF was observed between the different Child–Pugh classes (Figure 2). Table 4 displays the correlations between the liver disease grade, as assessed by the CPSs and MELD scores, and the analysed liver function parameters. The CPS had statistically significant negative correlations with total liver functional capacity (HEFml) and median HEF. The irBF had a statistically significant positive correlation with the CPS, whereas MTT did not seem to correlate at all in this study. The correlations described above are also exemplified and illustrated in the scatter plots of Figure 3. The MELD score had a negative correlation with total liver function (HEFml) and median HEF, but not with MTT or irBF. Liver function was statistically significantly more heterogeneously distributed in the patient group as shown in Figure 4. In healthy controls, the left hemiliver accounted for 34% of the volume and 33% of the function and the right hemiliver for 64% of the volume and 65% of the function (median values). This relationship was quite stable in the control group, as opposed to the patient group where large variations and predominantly left liver hypertrophy were observed, as illustrated in Figure 5. In healthy volunteers, the median HEF for the right liver was 0.22 and for the left liver was 0.20 ($p<0.05$). In the cirrhosis population this study suggests the opposite, with the median HEF being 0.8 for the right liver and 0.11 for the left liver, but the difference was not statistically significant ($p=0.06$).

DISCUSSION

This study demonstrates a novel method to assess total and regional liver function using DHCE-MRI. It shows that DHCE-MRI-derived liver function parameters differ between patients with liver cirrhosis and healthy controls. Furthermore, DHCE-MRI-derived functional

Figure 2. Liver perfusion assessed by input-relative blood flow (irBF). Liver perfusion seems to increase with disease severity graded according to Child–Pugh class as shown in this box plot. Dots outside the plot indicate outliers. There was only one observation with Child–Pugh class, and it is hence represented by a line only.

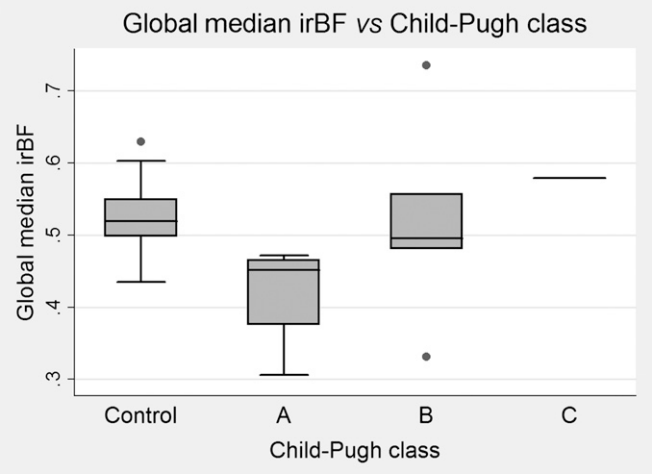

Table 4. Correlation of liver function parameters and scoring models

	CPS		MELD	
	Spearman ρ	p-value	Spearman ρ	p-value
Total functional capacity (HEFml)	−0.72	<0.05	−0.76	<0.05
Global median HEF	−0.80	<0.05	−0.73	<0.05
Global median irBF	0.76	<0.05	0.55	0.10
Global median MTT	−0.26	0.46	0.05	0.88

CPS, child-pugh score; HEF, hepatic extraction fraction; irBF, input-relative blood flow; MELD, model for end-stage liver disease; MTT, mean transit time.

parameters correlate well with the disease severity as staged by the CPSs and MELD scores. More importantly, the study demonstrates a non-homogeneous distribution of function within the liver in cirrhotic patients, unrelated to changes in volume. Hypertrophy of the left hemiliver in cirrhotic patients is a well-described phenomenon, a finding that was reproduced in our study [38–41]. The study also implied an improved quality of the hypertrophied left liver, in terms of function, compared with the right liver, although this finding was not statistically significant.

The lower HEF and HEFml in the patient group can be explained by a reduced functional hepatocyte mass or hepatocytes with less capacity to transport gadoxetate across the hepatocyte membrane compared with healthy liver parenchyma. The shorter MTT seen in the patient group could be owing to a larger proportion of the contrast agent being washed out of the system through the vascular outflow. In healthy livers, the longer MTT could be the result of uptake into hepatocytes, intracellular transport and subsequent biliary excretion, a process that is undoubtedly more time-consuming. The increasing irBF, as seen in Figure 2, could be interpreted as the result of the arterialisation that cirrhotic liver parenchyma has been shown to undergo with increasing disease severity [42].

Some of the variations in the functional parameters described in this work could be attributed to motion artefacts and partial volume effects. Even though individual voxels are small, they will inevitably include

Figure 3. Correlation of Child–Pugh score (CPS) and liver function parameters. A strong and statistically significant correlation between the CPS and all liver function parameters derived from deconvolutional analysis, except mean transit time, was observed. HEF, hepatic extraction fraction; irBF, input-relative blood flow; MTT, mean transit time.

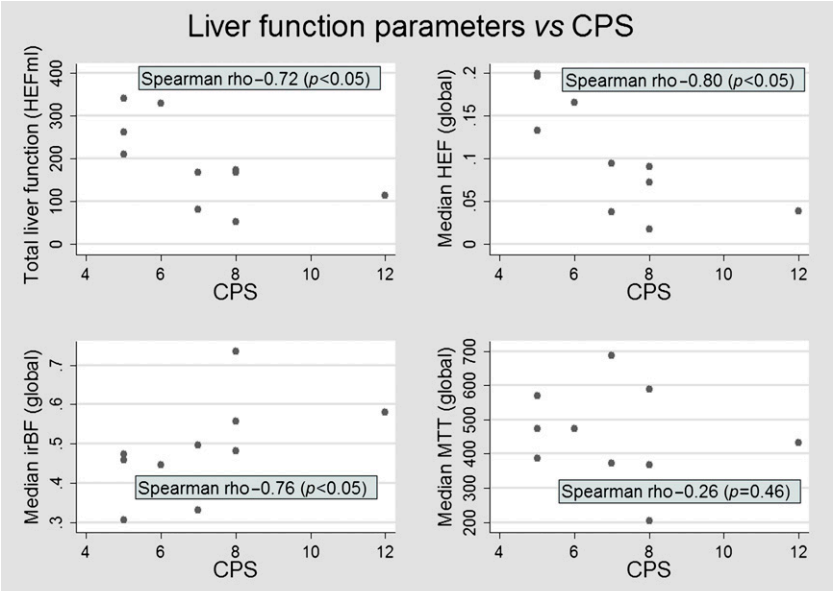

Figure 4. Distribution of incongruence score (IS) in patients and controls. Liver function was more inhomogeneously distributed among patients with a median IS of 2.7 (range 0.6–25.3) as compared with 0.4 (range 0.1–1.1) among controls ($p<0.05$).

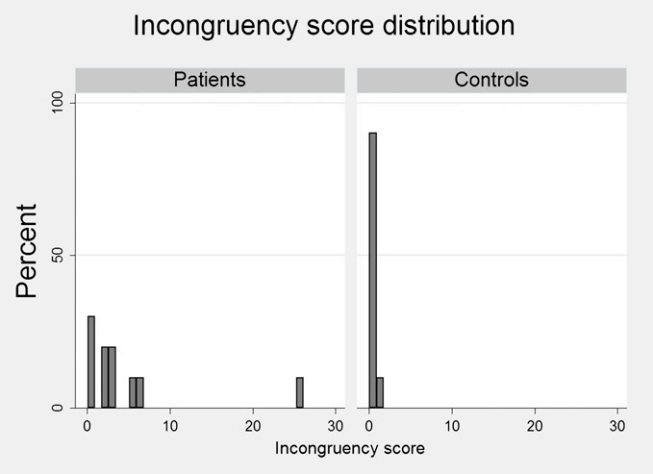

Figure 5. The distribution of function and volume in the right and left hemilivers. A box-plot of the function and volume distribution in the patient and control group. Note the large variations in liver function and volumes in the patient group, with one patient having >60% of the total liver function in the left hemiliver and <30% of the function in the right hemiliver. A single dot outside the box plot represents an outlier.

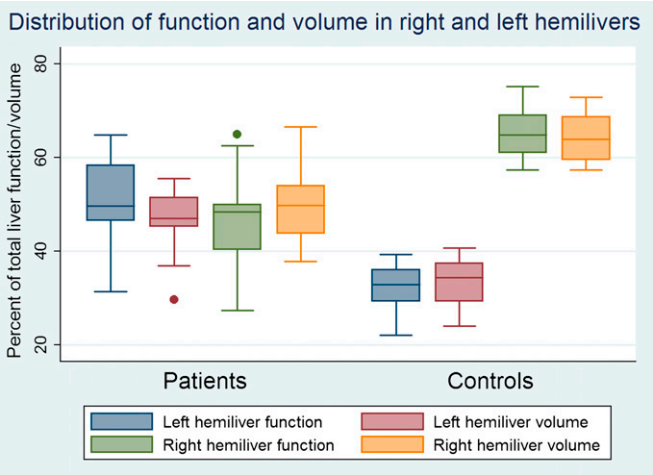

varying volumes of non-hepatocyte tissue. Conceptually, an ROI or a voxel containing a higher proportion of vessels would yield a higher irBF owing to higher perfusion and a lower HEF since extraction only takes place in hepatocytes. The reverse would be the case in a voxel or an ROI containing a higher proportion of hepatocytes. To minimise this, voxels with irBF above a user-defined threshold were omitted from analysis since they were regarded as mainly representing vascular tissue. Voxels close to liver boundaries are also prone to partial volume effects and to a varying degree contain non-liver tissue, which of course influences both calculation of functional parameters and the accuracy of liver volume estimations. Correction for motion artefacts using image registration algorithms before image analysis would be a logical next step in improving the method.

In this study, the patient group was markedly older than the controls and gender distribution was not proportional. It could be argued that the differences described should be attributed to these baseline differences regarding the groups rather than cirrhosis. This is an issue that needs to be addressed in further studies that, preferably, should be randomised or at least better matched for baseline characteristics.

In patients with diseased liver, the combination of volume-based and global function-based methods to estimate post-operative liver function could be unreliable owing to the inhomogeneous distribution of function as shown in this study. Segmental function measurements should probably be added to the equation in order to improve the prediction of post-operative remnant liver function, thereby lowering the risk of often fatal post-operative liver failure.

Historically, underlying parenchymal liver disease in patients considered for liver resection was almost exclusively limited to cirrhosis in patients with HCC. Today colorectal cancer liver metastases have, at least in Western countries, become the most common indication for liver resection, and chemotherapy is used with increasing frequency for down-staging or in neoadjuvant settings. Although not all agents have been studied, some have shown to be hepatotoxic, resulting in sinusoidal obstruction syndrome and chemotherapy-associated steatohepatitis, associated with a higher morbidity and in some cases even mortality after surgery [1,43]. Non-alcoholic fatty liver disease has become the most common chronic liver disease in the Western world, with between 10% and 20% of the patients progressing to non-alcoholic steatohepatitis, which may in turn lead to liver cirrhosis [44–46]. In current practice, parenchymal dysfunction is encountered with increasing frequency in non-cirrhotic patients, and both chemotherapy-induced liver injury

and metabolic syndrome-associated hepatic disease have been shown to be unevenly distributed in the liver [47–49].

There are several limitations to this study, the most important being the low number of participating subjects, the lack of specific inclusion and exclusion criteria and the lack of a reference method to correlate the DHCE-MRI results against. The study results should therefore be regarded with some caution, although the results are encouraging enough to warrant further studies, and the results from this work could serve as the basis for power calculations in future studies.

In conclusion, this study describes the application of DHCE-MRI in patients with cirrhosis showing correlation of DHCE-MRI-derived parameters with disease severity. It furthermore demonstrates the heterogeneous nature of liver disease and points towards the necessity of a segmental liver function test in functional assessment of patients with liver disease.

FUNDING

Financial support was provided through the regional agreement on medical training and clinical research (ALF) between the Stockholm county council and Karolinska Institutet, by the Ruth and Richard Juhlin Foundation, Karolinska Institutet and through research grants from Karolinska Institutet.

CONFLICT OF INTEREST

Henrik Nilsson, Eduard Jonas and Lennart Blomqvist have received consultancy fees from Bayer AG. Lennart Blomqvist is also a member of Primovist Advisory Board sponsored by Bayer AG.

REFERENCES

1. Mullen JT, Ribero D, Reddy SK, Donadon M, Zorzi D, Gautam S, et al. Hepatic insufficiency and mortality in 1,059 noncirrhotic patients undergoing major hepatectomy. J Am Coll Surg 2007; 204:854–62. doi: 10.1016/j.jamcollsurg.2006.12.032; discussion 62–4.
2. Capussotti L, Vigano L, Giuliante F, Ferrero A, Giovannini I, Nuzzo G. Liver dysfunction and sepsis determine operative mortality after liver resection. Br J Surg 2009;96: 88–94. doi: 10.1002/bjs.6429.
3. Balzan S, Belghiti J, Farges O, Ogata S, Sauvanet A, Delefosse D, et al. The "50-50 criteria" on postoperative day 5: an accurate predictor of liver failure and death after hepatectomy. Ann Surg 2005;242:824–8, discussion 28–9.
4. Sakamoto S, Uemoto S, Uryuhara K, Kim Id, Kiuchi T, Egawa H, et al. Graft size assessment and analysis of donors for living donor liver transplantation using right lobe. Transplantation 2001;71:1407–13.
5. Schroeder T, Radtke A, Kuehl H, Debatin JF, Malagó M, Ruehm SG. Evaluation of living liver donors with an all-inclusive 3D multidetector row CT protocol. Radiology 2006;238:900–10. doi: 10.1148/radiol.2382050133.
6. Morris-Stiff G, Gomez D, Prasad R. Quantitative assessment of hepatic function and its relevance to the liver surgeon. J Gastrointest Surg 2009;13:374–85. doi: 10.1007/s11605-008-0564-1.
7. Stockmann M, Lock JF, Malinowski M, Niehues SM, Seehofer D, Neuhaus P. The LiMAx test: a new liver function test for predicting postoperative outcome in liver surgery. HPB (Oxford) 2010;12:139–46.
8. Child CG, Turcotte JG. Surgery and portal hypertension. Major Probl Clin Surg 1964;1:1–85.
9. Pugh RN, Murray-Lyon IM, Dawson JL, Pietroni MC, Williams R. Transection of the oesophagus for bleeding oesophageal varices. Br J Surg 1973;60:646–9.
10. Kamath PS, Kim WR. The model for end-stage liver disease (MELD). Hepatology 2007;45:797–805. doi: 10.1002/hep.21563.
11. de Graaf W, van Lienden KP, van Gulik TM, Bennink RJ. (99m)Tc-mebrofenin hepatobiliary scintigraphy with SPECT for the assessment of hepatic function and liver functional volume before partial hepatectomy. J Nucl Med 2010;51:229–36. doi: 10.2967/jnumed.109.069724.
12. Imaeda T, Kanematsu M, Asada S, Seki M, Doi H, Saji S. Utility of Tc-99m GSA SPECT imaging in estimation of functional volume of liver segments in health and liver diseases. Clin Nucl Med 1995;20: 322–8.
13. Matsuzaki S, Onda M, Tajiri T, Kim DY. Hepatic lobar differences in progression of chronic liver

disease: correlation of asialoglycoprotein scintigraphy and hepatic functional reserve. Hepatology 1997;25:828–32. doi: 10.1002/hep.510250407.
14. Jonas E, Näslund E, Freedman J, Befrits R, Blomqvist L, Siosteen AK, et al. Measurement of parenchymal function and bile duct flow in primary sclerosing cholangitis using dynamic 99mTc-HIDA SPECT. J Gastroenterol Hepatol 2006;21:674–81. doi: 10.1111/j.1440-1746.2005.04084.x.
15. Nassif A, Jia J, Keiser M, Oswald S, Modess C, Nagel S, et al. Visualization of hepatic uptake transporter function in healthy subjects by using gadoxetic acid-enhanced MR imaging. Radiology 2012;264:741–50. doi: 10.1148/radiol.12112061.
16. Leonhardt M, Keiser M, Oswald S, Kühn J, Jia J, Grube M, et al. Hepatic uptake of the magnetic resonance imaging contrast agent Gd-EOB-DTPA: role of human organic anion transporters. Drug Metab Dispos 2010;38:1024–8. doi: 10.1124/dmd.110.032862.
17. Narita M, Hatano E, Arizono S, Miyagawa-Hayashino A, Isoda H, Kitamura K, et al. Expression of OATP1B3 determines uptake of Gd-EOB-DTPA in hepatocellular carcinoma. J Gastroenterol 2009;44:793–8. doi: 10.1007/s00535-009-0056-4.
18. Kitao A, Zen Y, Matsui O, Gabata T, Kobayashi S, Koda W, et al. Hepatocellular carcinoma: signal intensity at gadoxetic acid-enhanced MR Imaging–correlation with molecular transporters and histopathologic features. Radiology 2010;256:817–26. doi: 10.1148/radiol.10092214.
19. Schuhmann-Giampieri G. Liver contrast media for magnetic resonance imaging. Interrelations between pharmacokinetics and imaging. Invest Radiol 1993;28:753–61.
20. de Graaf W, Hausler S, Heger M, van Ginhoven TM, van Cappellen G, Bennink RJ, et al. Transporters involved in the hepatic uptake of (99m)Tc-mebrofenin and indocyanine green. J Hepatol 2011;54:738–45. doi: 10.1016/j.jhep.2010.07.047.
21. Hamm B, Staks T, Mühler A, Bollow M, Taupitz M, Frenzel T, et al. Phase I clinical evaluation of Gd-EOB-DTPA as a hepatobiliary MR contrast agent: safety, pharmacokinetics, and MR imaging. Radiology 1995;195:785–92.
22. Kim T, Murakami T, Hasuike Y, Gotoh M, Kato N, Takahashi M, et al. Experimental hepatic dysfunction: evaluation by MRI with Gd-EOB-DTPA. J Magn Reson Imaging 1997;7:683–8.
23. Murakami T, Kim T, Gotoh M, Hasuike Y, Kato N, Miyazawa T, et al. Experimental hepatic dysfunction: evaluation by MR imaging with Gd-EOB-DTPA. Acad Radiol 1998;5:S80–2.
24. Ryeom HK, Kim SH, Kim JY, Kim HJ, Lee JM, Chang YM, et al. Quantitative evaluation of liver function with MRI Using Gd-EOB-DTPA. Korean J Radiol 2004;5:231–9.
25. Schmitz SA, Mühler A, Wagner S, Wolf KJ. Functional hepatobiliary imaging with gadolinium-EOB-DTPA. A comparison of magnetic resonance imaging and 153gadolinium-EOB-DTPA scintigraphy in rats. Invest Radiol 1996;31:154–60.
26. Yamada A, Hara T, Li F, Fujinaga Y, Ueda K, Kadoya M, et al. Quantitative evaluation of liver function with use of gadoxetate disodium-enhanced MR imaging. Radiology 2011;260:727–33. doi: 10.1148/radiol.11100586.
27. Motosugi U, Ichikawa T, Sou H, Sano K, Tominaga L, Kitamura T, et al. Liver parenchymal enhancement of hepatocyte-phase images in Gd-EOB-DTPA-enhanced MR imaging: which biological markers of the liver function affect the enhancement? J Magn Reson Imaging. 2009;30:1042–6.
28. Tschirch FT, Struwe A, Petrowsky H, Kakales I, Marincek B, Weishaupt D. Contrast-enhanced MR cholangiography with Gd-EOB-DTPA in patients with liver cirrhosis: visualization of the biliary ducts in comparison with patients with normal liver parenchyma. Eur Radiol 2008;18:1577–86.
29. Nilsson H, Blomqvist L, Douglas L, Nordell A, Jonas E. Assessment of liver function in primary biliary cirrhosis using Gd-EOB-DTPA-enhanced liver MRI. HPB (Oxford) 2010;12:567–76. doi: 10.1111/j.1477-2574.2010.00223.x.
30. Saito K, Ledsam J, Sourbron S, Otaka J, Araki Y, Akata S, et al. Assessing liver function using dynamic Gd-EOB-DTPA-enhanced MRI with a standard 5-phase imaging protocol. J Magn Reson Imaging 2012; in press. E-pub ahead of print october 2012. doi: 10.1002/jmri.23907.
31. Nilsson H, Nordell A, Vargas R, Douglas L, Jonas E, Blomqvist L. Assessment of hepatic extraction fraction and input relative blood flow using dynamic hepatocyte-specific contrast-enhanced MRI. J Magn Reson Imaging 2009;29:1323–31. doi: 10.1002/jmri.21801.
32. Desmet VJ, Gerber M, Hoofnagle JH, Manns M, Scheuer PJ. Classification

of chronic hepatitis: diagnosis, grading and staging. Hepatology 1994;19:1513–20.
33. Kamath PS, Wiesner RH, Malinchoc M, Kremers W, Therneau TM, Kosberg CL, et al. A model to predict survival in patients with end-stage liver disease. Hepatology 2001;33:464–70. doi: 10.1053/jhep.2001.22172.
34. Strasberg SM. Terminology of liver anatomy and liver resections: coming to grips with hepatic Babel. J Am Coll Surg 1997;184:413–34.
35. Strasberg SM. Nomenclature of hepatic anatomy and resections: a review of the Brisbane 2000 system. J Hepatobiliary Pancreat Surg 2005;12:351–5. doi: 10.1007/s00534-005-0999-7.
36. Dodds WJ, Erickson SJ, Taylor AJ, Lawson TL, Stewart ET. Caudate lobe of the liver: anatomy, embryology, and pathology. AJR Am J Roentgenol 1990;154:87–93.
37. Brown PH, Juni JE, Lieberman DA, Krishnamurthy GT. Hepatocyte versus biliary disease: a distinction by deconvolutional analysis of technetium-99m IDA time-activity curves. J Nucl Med 1988;29:623–30.
38. Blomquist L, Wang Y, Kimiaei S, Jacobsson H. Change in size, shape and radiocolloid uptake of the alcoholic liver during alcohol withdrawal, as demonstrated by single photon emission computed tomography. J Hepatol 1994;21:417–23.
39. Shreiner DP, Barlai-Kovach M. Diagnosis of alcoholic cirrhosis with the right-to-left hepatic lobe ratio: concise communication. J Nucl Med 1981;22:116–20.
40. Harbin WP, Robert NJ, Ferrucci JT Jr. Diagnosis of cirrhosis based on regional changes in hepatic morphology: a radiological and pathological analysis. Radiology 1980;135:273–83.
41. Torres WE, Whitmire LF, Gedgaudas-McClees K, Bernardino ME. Computed tomography of hepatic morphologic changes in cirrhosis of the liver. J Comput Assist Tomogr 1986;10:47–50.
42. Annet L, Materne R, Danse E, Jamart J, Horsmans Y, Van Beers BE. Hepatic flow parameters measured with MR imaging and Doppler US: correlations with degree of cirrhosis and portal hypertension. Radiology 2003;229:409–14. doi: 10.1148/radiol.2292021128.
43. Pawlik TM, Olino K, Gleisner AL, Torbenson M, Schulick R, Choti MA. Preoperative chemotherapy for colorectal liver metastases: impact on hepatic histology and postoperative outcome. J Gastrointest Surg 2007;11:860–8. doi: 10.1007/s11605-007-0149-4.
44. Pessaux P, Chenard MP, Bachellier P, Jaeck D. Consequences of chemotherapy on resection of colorectal liver metastases. J Visc Surg 2010;147:e193–201. doi: 10.1016/j.jviscsurg.2010.06.004.
45. Wieckowska A, McCullough AJ, Feldstein AE. Noninvasive diagnosis and monitoring of nonalcoholic steatohepatitis: present and future. Hepatology 2007;46:582–9. doi: 10.1002/hep.21768.
46. Arun J, Jhala N, Lazenby AJ, Clements R, Abrams GA. Influence of liver biopsy heterogeneity and diagnosis of nonalcoholic steatohepatitis in subjects undergoing gastric bypass. Obes Surg 2007;17:155–61. doi: 10.1007/s11695-007-9041-2.
47. Larson SP, Bowers SP, Palekar NA, Ward JA, Pulcini JP, Harrison SA. Histopathologic variability between the right and left lobes of the liver in morbidly obese patients undergoing Roux-en-Y bypass. Clin Gastroenterol Hepatol 2007;5:1329–32. doi: 10.1016/j.cgh.2007.06.005.
48. Merriman RB, Ferrell LD, Patti MG, Weston SR, Pabst MS, Aouizerat BE, et al. Correlation of paired liver biopsies in morbidly obese patients with suspected nonalcoholic fatty liver disease. Hepatology 2006;44:874–80. doi: 10.1002/hep.21346.
49. Ratziu V, Charlotte F, Heurtier A, Gombert S, Giral P, Bruckert E, et al. Sampling variability of liver biopsy in nonalcoholic fatty liver disease. Gastroenterology 2005;128:1898–906.